

Hierarchical Structures in Lamellar Hydrogen Bonded LC Side Chain Diblock Copolymers

Antti J. Soininen,[†] Ioanna Tanionou,[‡] Niels ten Brummelhuis,[§] Helmut Schlaad,[§] Nikos Hadjichristidis,^{*,‡} Olli Ikkala,[†] Janne Raula,[†] Raffaele Mezzenga,^{||} and Janne Ruokolainen^{*,†}

[†]Department of Applied Physics, Aalto University School of Science, 02150 Espoo, Finland

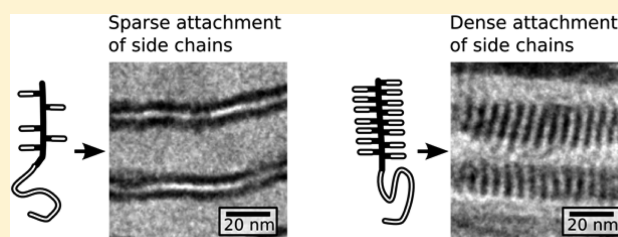
[‡]Laboratory of Industrial Chemistry, Department of Chemistry, National and Kapodistrian University of Athens, 15784 Athens, Greece

[§]Department of Colloid Chemistry, Max Planck Institute of Colloids and Interfaces, Research Campus Golm, 14424 Potsdam, Germany

^{||}Food & Soft Materials, Department of Health Science & Technology, ETH Zurich, 8092 Zürich, Switzerland

S Supporting Information

ABSTRACT: We show that in a hydrogen bonded LC side chain diblock copolymer with lamellar morphology on the block copolymer level, two distinct packing mechanisms of the side chain blocks are possible depending on the amount of hydrogen bonded side chains. We mixed a hydrogen bonding mesogen, cholesteryl hemisuccinate (CholHS), with poly(1,2-butadiene)-*block*-poly(2-vinylpyridine) (PBd-P2VP) and poly(styrene)-*block*-poly(4-vinylpyridine) (PS-P4VP), in which the poly(vinylpyridine) act as host blocks, and we varied the CholHS to pyridine repeat unit ratio (x). With all x , a lamellar morphology on the block copolymer level was achieved. However, at low binding of CholHS to the host block, the CholHS side chains microphase separated into a single layer inside the poly(pyridine) lamellae resulting in a novel microphase separated structure. This includes, for example, the PS-P4VP sample with $x = 0.25$ and all the PBd-P2VP based samples since hydrogen bonding of CholHS to P2VP was sterically limited as revealed by infrared spectroscopy. No such limits were present in the rest of the PS-P4VP samples which showed a gradual shift from the single CholHS lamella morphology to exclusively liquid crystalline smectic layers oriented perpendicular to the block domain interfaces.



INTRODUCTION

Comb-coil type diblock copolymers with a coil block and a side chain grafted block can form hierarchical structure-within-structure type morphologies where the copolymer blocks microphase separate in a 10–100 nm length scale, while the side chain blocks organize in a 1–10 nm length scale domains within the microphase separated block copolymer structure.^{1–3} In the usual case, the side chain blocks form liquid crystalline (LC) smectic layers perpendicular to the block domain interfaces. The side chains themselves do not need to be liquid crystalline, however. The smectic layer formation has been observed in several systems where nonliquid crystal side chains are physically attached to the host block of a diblock copolymer.^{4–10}

In linear block copolymer systems, the microphase separated morphology depends mainly on the relative volumes of the blocks while the periodicity of the morphology depends on the total length of the copolymer chains. For the ideal coil-coil diblock copolymer case, the phase diagram is symmetric: the microphase separated structure is inverted if the volume fractions of the blocks are reversed. This changes, however, when side chains are attached to one of the blocks. Theoretical studies^{11–13} predict that in side chain block copolymers, the

coil block is confined in cylindrical domains at higher volume fractions than in the coil-coil case. Also, the increased energetic cost of confining the side chain block in domains with curved interfaces extends the lamellar phase until relatively low volume fractions of the side chain block. This shift of the boundaries of morphologies in the phase diagram can be explained by the liquid crystalline nature and increased effective cross sectional area of the side chain block compared to the coil block, which has been also confirmed experimentally.^{14–20} An example of the interplay between the side chains and the polymer blocks is provided by Anthamatten et al.^{18,21} who studied a series of side chain LC diblock copolymers with a poly(styrene)-*block*-poly(methacrylate) backbone. They encountered perforated lamellae or mixed cylindrical/lamellar morphologies with nearly symmetrical composition (weight fraction) where a purely lamellar morphology would be expected for simple coil-coil diblock copolymers. The mixed cylindrical/lamellar morphology reversibly transformed to a purely lamellar morphology upon heating. This loss of

Received: April 23, 2012

Revised: August 9, 2012

Published: August 30, 2012



curvature was attributed to the collapse of the liquid crystalline ordering of the side chains and subsequent decrease in the cross sectional area of the side chain block. Further, with shorter side chain block lengths, the lamellar to disordered morphology transition was triggered by the isotropization of the LC side chains. This exemplifies the competition between liquid crystalline ordering of the side chains and the microphase separation of the polymeric backbone. The competition can be exploited to direct the microphase separation in thin films (see, for example, the review by Yu et al.²²). Basically the microphase separated structure of a block copolymer in confined geometry is determined by the shape of the confinement and its surface energy. In thin films, this usually leads to structures oriented parallel to the film surfaces due to lower surface energy of one of the blocks. However, the tendency of the side chains to form smectic layers also parallel to the film interfaces may overcome the preferential orientation of the microphase separated structures of the block copolymer backbone and orient the larger structures perpendicularly to the film surfaces.

Attachment of the side chains by weak physical bonds like the hydrogen bond allows control over the number of side chains bonded to a polymer backbone.²³ This directly influences the volume fraction of the side chain block. As an example, Bondzic et al. have studied octyl gallate hydrogen bonded to the pyridine groups of poly(isoprene)-*block*-poly(2-vinylpyridine) (PI-P2VP) and poly(isoprene)-*block*-poly(4-vinylpyridine) (PI-P4VP).⁷ The pure PI-P4VP did not show any microphase separated structure, but after addition of octyl gallate, P4VP(octyl gallate) cylinders in PI matrix were found with fairly low volume fractions of the P4VP(octyl gallate) block. However, the more interesting case was that of PI-P2VP(octyl gallate). First, at lower fractions of octyl gallate side chains to P2VP repeat units, the cylindrical morphology was found as in the case of the PI-P4VP backbone, but at octyl gallate to P2VP repeat unit ratio of one, the morphology changed to lamellar. However, the total volume fraction of P2VP(octyl gallate) was still rather low (about 0.3) for the lamellar morphology but in agreement with the theoretical treatments discussed above. Heating the sample led to reversible lamellar to cylindrical phase transition due to thermal breaking of the hydrogen bonds between octyl gallate and P2VP and subsequent coiling of the block.²⁴ The reversibility of the weak physical bonds has been studied also with 3-pentadecyl phenol hydrogen bonded to poly(styrene)-*block*-poly(4-vinylpyridine)²⁵ (PS-P4VP), with dodecylbenzenesulphonic acid bonded to poly(butadiene)-*block*-poly(ethylene oxide)²⁶ or with 4-hydroxyphenylacetamide bonded to PS-P2VP.²⁷ The phenomenon can be utilized to create functional block copolymer materials with switchable properties like electrical conductivity²⁸ or photonic band gap.^{29,30}

As stated earlier, usually the side chain blocks organize in smectic lamellae perpendicular to the block copolymer domain interfaces. Parallel alignment of the smectic layers can be achieved with external driving forces, such as roll casting^{18,31} or shear alignment.^{32,33} In the case of bent core mesogens hydrogen bonded to PS-P4VP, parallel smectic layers formed inside the P4VP domains after shearing.³² The authors argued that the parallel alignment was due to the low attachment ratio of the mesogens (one mesogen in every ten repeat units): the attached and nonattached parts of the P4VP chains would “microphase separate” into lamellar subphase inside the P4VP domains due to repulsion between the parts behaving like multiblock copolymers. It is interesting to note, that the

lamellar period of the whole block copolymer structure decreased upon the side chain attachment. The exact opposite would be expected since molecules were added to the system. The decrease was explained by stretching of the P4VP chains and subsequent decrease in the thickness of the parallel lamellar subphase.

Usually, the morphology of coil-side chain diblock copolymers change as additional side chains are attached to the copolymer. However, in this study, the relative block lengths of the block copolymer backbones were selected such that lamellar microphase separated structures could be expected within the range of side chains to host block repeat unit ratios used. The aim of this work was to investigate the influence of the amount of side chains on the side chain subphase structure in a systematic manner while maintaining the fixed lamellar morphology at the block copolymer level. Further, the bonding of side chains to a polymeric backbone may play a role in the formation of the subphase. We will show evidence of a new side chain block structure found at low amounts of hydrogen bonded side chains which is different from the usual lamellar-within-lamellar structures and which, to our knowledge, has not been reported before. In this study, two diblock copolymers, poly(1,2-butadiene)-*block*-poly(2-vinylpyridine) (PBd-P2VP) and poly(styrene)-*block*-poly(4-vinylpyridine) (PS-P4VP), were used as backbones for cholesteryl hemisuccinate (CholHS) side chains. The fundamental difference between the P2VP and P4VP blocks is the position of the hydrogen bonding site in the pyridine ring. In P2VP the site is not readily accessible which sterically hinders the hydrogen bonding of CholHS. Thus, in addition to the amount of side chains compared to binding sites in the polymeric backbones, the effect of the bonding of the side chains to the formation of the subphase domain is investigated.

■ EXPERIMENTAL SECTION

Materials. The synthesis of PBd-P2VP was based on sequential addition of monomers via anionic polymerization method. THF, which was used as the solvent for the reactions, was purified with *sec*-butyllithium to prevent side reactions during the polymerization of PBd which was carried out at $-20\text{ }^{\circ}\text{C}$. Subsequent polymerization of the P2VP block was carried out at $-78\text{ }^{\circ}\text{C}$ to avoid termination phenomena. The molecular mass in the final product for the PBd block was 15,000 g/mol and for the P2VP block 4,000 g/mol, while the polydispersity index (PDI) was 1.03 according to size exclusion chromatography. According to ^1H NMR, 89% of the PBd repeat units were of the 1,2 addition. See the Supporting Information for details on the synthesis and characterization.

PBd-P2VP, PS-P4VP (PS block: 31,900 g/mol, P4VP block: 13,200 g/mol, PDI: 1.08, Polymer Source), and CholHS (molecular weight: 486.73 g/mol, Sigma-Aldrich) were dried overnight in a vacuum oven before use. CholHS was dissolved as 1 w% solution in tetrahydrofuran (THF, Sigma-Aldrich) dried by molecular sieves (Fluka). Then PBd-P2VP and PS-P4VP were dissolved into the CholHS solution to obtain liquid crystal side chain diblock copolymers at different CholHS to pyridine ratios which were 0.25, 0.40, 0.50, 0.60, and 0.75 for PBd-P2VP and 0.25, 0.50, and 0.75 for PS-P4VP. After a few hours of mixing, the solutions were left to evaporate. Then annealing was performed in 3 bar nitrogen atmosphere at $160\text{ }^{\circ}\text{C}$ for three days for PS-P4VP(CholHS) and four days for PBd-P2VP(CholHS).

Infrared Spectroscopy. For Fourier transform infrared (FTIR) spectroscopy, the PBd-P2VP(CholHS) samples, pristine PBd-P2VP and pristine CholHS, were embedded in potassium bromide (Fluka) pellets. The measurements were carried out on a Nicolet 380 spectrometer (Thermo Fisher Scientific) in transmission mode with 2 cm^{-1} resolution and averaging over 64 scans. Areas under absorbance

peaks were calculated by subtracting a polynomial baseline and fitting Lorentzian shaped functions to the peaks using the Fityk software.³⁴

Nuclear Magnetic Resonance Spectroscopy. Nuclear magnetic resonance spectra of diluted solutions of PBd-P2VP in deuterated chloroform were taken in a Varian Unity Plus 300/54 device at room temperature.

Size Exclusion Chromatography. Size exclusion chromatography was applied on PBd-P2VP using a Waters 610 pump and a differential refractometer Waters 410 as a detector. Four μ -Styragel type columns with porous material (pore size 10^2 to 10^6 Å) were also used. The measurements were done at 40 °C in THF with flow of 1 mL/min.

Small Angle X-ray Scattering. The samples (about 1 mm thick in the beam direction) were maintained between two Kapton films for small-angle X-ray scattering (SAXS) measurements. The device consisted of MICROSTAR microfocus rotating anode X-ray source (Bruker) with Montel Optics (copper K_{α} radiation, wavelength $\lambda = 1.54$ Å, Incoatec). The beam was further collimated to a diameter of approximately 1 mm at the sample position using four sets of four blade slits (JJ X-ray). Sample-to-detector distance of about 160 cm was used, except for pristine PBd-P2VP, where sample-to-detector distance was about 260 cm. The scattering intensities were measured using a HiStar 2-D area detector (Bruker). The spatially corrected two-dimensional scattering images were integrated in the radial direction to obtain the magnitude of scattering vector vs intensity curves. The magnitude of the scattering vector q is given by $q = 4\pi \sin(\theta)/\lambda$, where θ is half of the scattering angle. The length of the lattice vector $a = 2\pi/q_1$ for lamellar systems where q_1 is the magnitude of the scattering vector at the first order scattering peak; for cylindrical hexagonal systems the length of the lattice vector $a = 4\pi/(\sqrt{3}q_1)$.

Transmission Electron Microscopy. Transmission electron microscopy (TEM) was carried out using JEM 3200FSC field emission microscope (Jeol) operated at 300 kV in bright field mode. The images were acquired with Ultrascan 4000 CCD camera (Gatan), while the specimen temperature was maintained at -187 °C. Additional imaging was done with Tecnai 12 microscope (FEI) equipped with Ultrascan 1000 CCD camera (Gatan). This microscope was operated at 120 kV in bright field mode. Thin sections (approximately 70 nm) of PBd-P2VP based samples were cut at -100 °C, and the sections were collected on 300 mesh lacey carbon grids. PS-P4VP based samples were cut at room temperature by Ultracut UTC microtome (Leica) using a 35° diamond knife (Diatome) and collected on 600 mesh copper grids. The samples were stained in vapor of iodine for four hours except pure PBd-P2VP which was stained in vapor of ruthenium tetroxide for 15 min. Iodine selectively stains the P2VP or P4VP blocks which renders the poly(pyridine) domains dark in bright field TEM images, while ruthenium tetroxide stains the PBd blocks.

RESULTS AND DISCUSSION

Molecular structures of the diblock copolymers and CholHS as well as their hydrogen bonding are shown in Figure 1. The key parameters of the samples [i.e., CholHS to pyridine ratios, weight fractions of the side chain blocks, lattice vector lengths (a) determined by SAXS and morphology according to TEM] are summarized in Table 1. The determination of the structures will be discussed later in the text in detail; first, the hydrogen bonding according to the results of FTIR measurements will be discussed.

Hydrogen Bonding of CholHS. Changes in certain IR absorption bands of the pyridine or CholHS indicate hydrogen bonding between the poly(vinylpyridine) blocks and the carboxyl group ($-\text{C}(\text{O})\text{OH}$) of the CholHS side chains. IR absorption can also be used to quantify the amount of dimerized CholHS which was not bonded to the backbone. The hydrogen bonding of CholHS to a P4VP backbone has

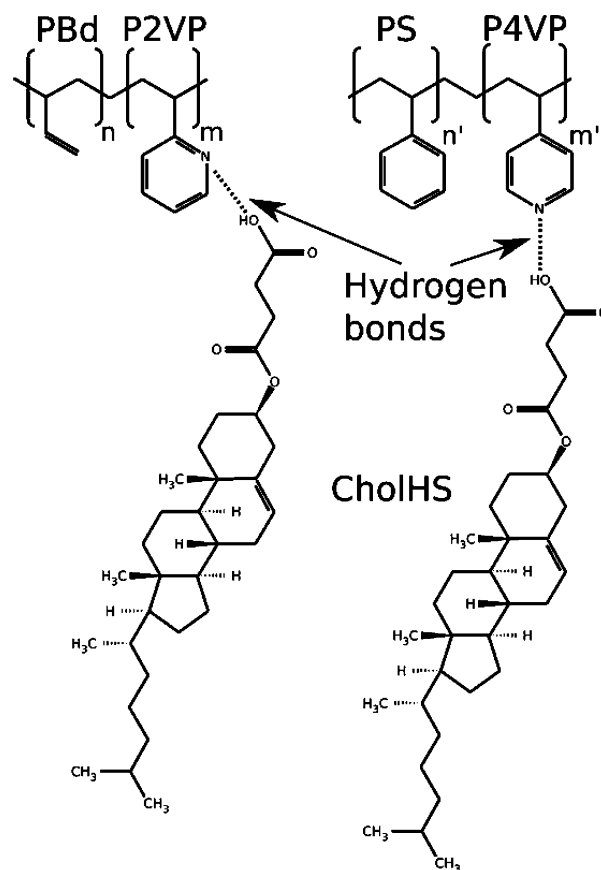


Figure 1. Molecular structures of PBd-P2VP (left) and PS-P4VP (right) block copolymers and CholHS mesogens. The CholHS mesogens associate with the nitrogen in the pyridine rings of the P2VP and P4VP blocks by hydrogen bonding.

Table 1. Properties PBd-P2VP(CholHS) and PS-P4VP(CholHS) Samples Investigated in This Study

backbone	sample	CholHS to pyridine ratio	weight fraction of the side chain block	microphase separated morphology (TEM)	length of lattice vector a (SAXS) (nm)
PBd-P2VP	P2 ^a	0.00	0.21	cylindrical	31.4
	P2-25	0.25	0.36	perforated lamellar	24.1
	P2-40	0.40	0.43	lamellar	25.9
	P2-50	0.50	0.47	lamellar	25.1
	P2-60	0.60	0.50	lamellar	25.1
	P2-75	0.75	0.54	lamellar	25.9
	P4 ^a	0.00	0.29	cylindrical	42.3
PS-P4VP	P4-25	0.25	0.47	lamellar	29.5
	P4-50	0.50	0.58	lamellar	29.5 and 36.0
	P4-75	0.75	0.65	lamellar	36.0

^aPure block copolymer.

been investigated before by Korhonen et al.¹⁰ Thus, only the case of P2VP will be discussed here in detail.

The two main regions of the FTIR spectra that concern the hydrogen bonding of CholHS to P2VP are shown in Figure 2. The lower wavenumber band at $1575\text{--}1615\text{ cm}^{-1}$, the right-hand side of Figure 2, shows absorption associated with the pyridine rings³⁵ only, since the PBd block does not absorb at these wavenumbers.³⁶ The absorption peak at 1590 cm^{-1} is due

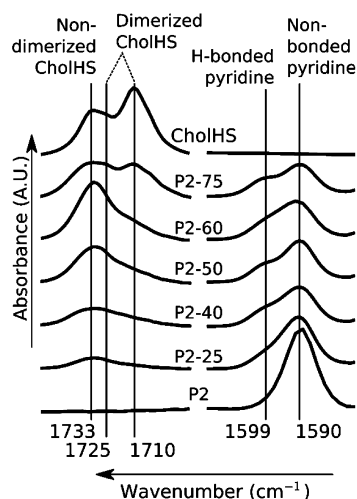


Figure 2. FTIR absorbance spectra of pristine CholHS, PBd-P2VP, and PBd-P2VP(CholHS) samples. The higher wavenumber band (1680–1760 cm^{-1}) on the left shows the fraction of dimerized CholHS in the samples, while the lower wavenumber band (1575–1615 cm^{-1}) on the right shows the ratio between hydrogen bonded and nonbonded pyridine groups of P2VP.

to non-hydrogen bonded pyridine, while the peak at 1599 cm^{-1} is due to hydrogen bonded pyridine. The fraction of P2VP repeat units hydrogen bonded to the CholHS side chains x_{HB} can be estimated using the ratio between the hydrogen bonded peak area A_{1599} and the total area of both peaks: $x_{\text{HB}} = A_{1599} / (A_{1599} + A_{1590})$.³⁷ This rough calculation shows that the fraction of hydrogen bonded P2VP repeat units saturates at around $x_{\text{HB}} \approx 0.3$. It should be noted that macrophase separation in the current PBd-P2VP(CholHS) system was evident only when the CholHS to P2VP unit ratio was 1.00 or higher (data not included here). This indicates that the nonattached CholHS mesogens dissolve into the attached CholHS domains which is reminiscent of the case of 4-(*n*-octyl)benzoic acid attached to P2VP and P4VP homopolymers.^{38,39}

Instead of bonding to the P2VP host block, part of the CholHS mesogens hydrogen bond with each other via dimerization of the carboxylic acid groups. In the dimerized state, the hydroxyl (–OH) group of the carboxylic acid group of a CholHS mesogen is hydrogen bonded to the carbonyl (>C=O) group of another CholHS. The dimerization can be investigated with FTIR using the carbonyl absorption peaks at the higher wavenumber band at 1680–1760 cm^{-1} shown on the left-hand side of Figure 2. The highest wavenumber peak at 1733 cm^{-1} is assigned to carbonyls, that is, non-hydrogen bonded or dimerized CholHS mesogens.⁴⁰ This includes both CholHS hydrogen bonded with the pyridine rings of P2VP via the hydroxyl group (–OH) and CholHS not hydrogen bonded at all. The absorption peaks at 1725 cm^{-1} and 1710 cm^{-1} , on the other hand, are assigned to the dimerized CholHS.⁴⁰ As can be seen from Figure 2, these peaks appear at every PBd-P2VP(CholHS) sample. The dimerization is another indicator that not all CholHS mesogens are hydrogen bonded to the P2VP blocks. The limited hydrogen bonding of CholHS to P2VP is in contrast with P4VP, where no such limitation was evident.¹⁰ In P2VP, the unfavorable positioning of the nitrogen atoms causes steric hindrance and limits the amount hydrogen bonded CholHS side chains to approximately one in three P2VP repeat units.

Structural Analysis of PBd-P2VP Based Samples. The microphase separated structures of the PBd-P2VP based samples were studied by SAXS which gives the lattice vector lengths a of the structures. The SAXS results and microphase separated morphologies were further confirmed by TEM. The pure PBd-P2VP sample P2 self-assembles in P2VP cylinders hexagonally arranged in PBd matrix as evident by the SAXS data shown in Figure 3 and the TEM image shown in Figure 4a.

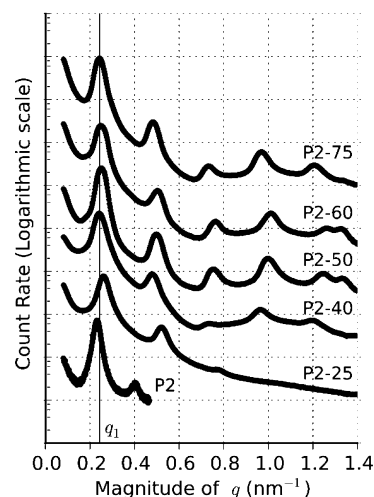


Figure 3. SAXS intensity curves of the PBd-P2VP and PBd-P2VP(CholHS) samples.

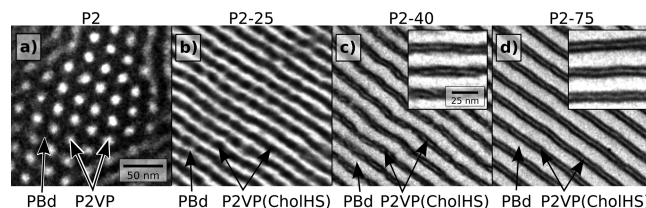


Figure 4. TEM images of PBd-P2VP based samples. a) Pure PBd-P2VP, P2, hexagonal arrangement of cylindrical P2VP domains (bright) in PBd matrix (dark, ruthenium tetroxide staining). b) P2-25, perforated lamellar morphology of PBd (bright) and P2VP(CholHS) (dark, iodine staining). c) P2-40, and d) P2-75, pure lamellar morphology; insets show a magnified view of the single CholHS layer inside the P2VP domains (thin white stripe inside the dark P2VP lamellae). The 50 nm scale bar is common to all four images, and the 25 nm scale bar is common to both insets.

The second order SAXS peak of P2 is located at $3^{1/2}$ times the position of the first order peak which is characteristic for hexagonal morphology. In TEM, the hexagonal cylindrical morphology is also evident. This morphology is expected, since the weight fraction of the P2VP block, 0.21, is within the cylinder forming region.

All the PBd-P2VP based samples with the CholHS side chains had evenly spaced SAXS peaks as shown in Figure 3. The spacing is characteristic for lamellar morphology. The transition from a cylindrical to lamellar microphase separated structure can be attributed to the increase in volume fraction of the P2VP(CholHS) blocks in the whole block copolymer. The TEM image of the PBd-P2VP sample containing the least CholHS, P2-25, shown in Figure 4b, however, reveals white ribbons connecting the PBd lamellae within the P2VP-(CholHS) regions (stained dark by iodine), which suggests that the structure may not be purely lamellar, but rather a

perforated lamellar, a metastable transient structure known to occur between cylindrical and lamellar structures and reported in many works since the early report by Matsuo et al.⁴¹ In this sample, there were no signs of organization of the CholHS mesogens in SAXS or in TEM which was probably due to the low amount of CholHS in the sample.

The PBd-P2VP(CholHS) samples with higher amount of CholHS were identified as lamellar without any signs of perforation. Instead, the CholHS mesogens were organized in a single layer parallel to the block domain interfaces, as shown in Figure 4c and d. The CholHS rich layers can be identified as the thin white stripes inside the dark P2VP domains in the TEM images in Figure 4c for P2-40 and in Figure 4d for P2-75. It should be noted, however, that although this structure was predominant in the samples, in TEM it was occasionally possible to come across small domains (about a hundred nanometers) of P2VP(CholHS) blocks organized in perpendicular smectic layers even after thermal annealing. These smectic “defects” can explain the small SAXS peaks at 1.33 nm^{-1} (which corresponds to mesogen spacing of 4.7 nm) shown in Figure 3. The low intensity of these peaks also suggests that the perpendicular smectic defects are only a minority, while the major part of CholHS mesogens is in the single layered subphases.

Structural Analysis of PS-P4VP Based Samples. The even spacing of the SAXS peaks of the pure PS-P4VP sample P4 shown in Figure 5 points to lamellar morphology. However,

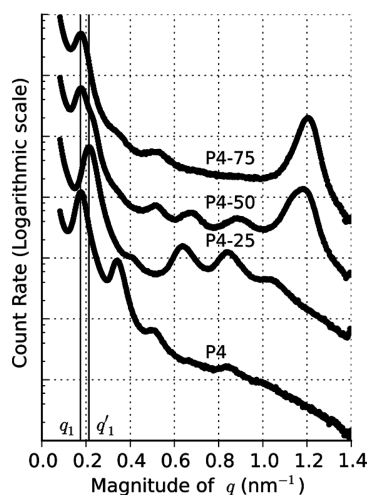


Figure 5. SAXS intensity curves of the PS-P4VP and PS-P4VP(CholHS) samples.

according to the P4VP block weight fraction of 0.29, a hexagonal morphology is expected, and, indeed, this is the case: the TEM image in Figure 6a shows P4VP cylinders in PS matrix. The missing hexagonal peaks in the SAXS curve are probably due to local minima in the form factor of this particular cylindrical structure.

The SAXS curves of P4-25 and P4-75 in Figure 5 shows the evenly spaced peaks although the second order peaks have relatively low intensity. It is worth noting, that the “intermediate” sample P4-50 combines the peaks of both P4-25 and P4-75. The TEM image of P4-25 in Figure 6b shows the same single layered CholHS subphase as the P2-40 and P2-75 samples shown in Figure 4c and d. In the sample containing the highest amount of CholHS, P4-75, however, the P4VP(CholHS) blocks organize into a lamellar-within-lamellar type

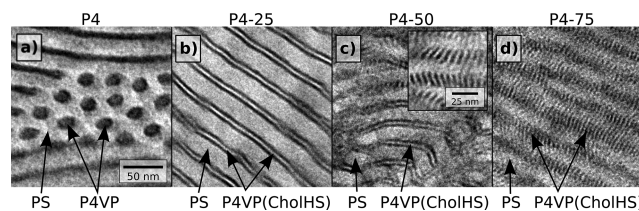


Figure 6. TEM images of PS-P4VP based samples. a) P4, hexagonal arrangement of cylindrical P4VP domains (dark, iodine staining) in PS matrix (bright). b) P4-25, lamellar morphology of PS (bright) and P4VP(CholHS) (dark/bright/dark due to iodine staining); thin bright CholHS layer between two dark P4VP layers. c) P4-50, lamellar morphology, side chain domain subphase partly changed to perpendicular smectic layers. d) P4-75, lamellar morphology, exclusively smectic side chain domain subphase. The 50 nm scale bar is common to all four images.

structure where smectic domains are perpendicular to the block copolymer domain interfaces. The high intensity SAXS peak at 1.20 nm^{-1} of P4-75 in Figure 5 corresponds to a period of 5.2 nm of these smectic layers. The difference with the 4.7 nm period of the smectic “defects” of PBd-P2VP(CholHS) is probably because of slightly different organization in the molecular level due to differences in hydrogen bonding between P2VP and P4VP. Interestingly, in P4-50 both the single layered CholHS and the perpendicular smectic structures can be found. This explains the mixed nature of the SAXS curve of P4-50 in Figure 5. The widening of the smectic peak around 1.2 nm^{-1} compared to P4-75 indicates less ordering.

Packing of the CholHS Subphase. Figure 7 shows schematically the arrangement of the two hierarchical lamellar structures. In both cases, the coil block and the side chain block microphase separate into their own lamellae at the block copolymer level. The spacing of the lamellae is measured in tens of nanometers at this level. With low hydrogen bonding of

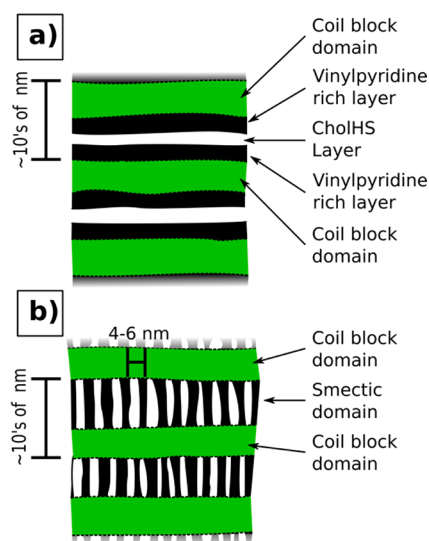


Figure 7. Single CholHS layer vs perpendicular smectic subphase in lamellar coil-side chain diblock copolymers. a) In the single layer packing, observed with low amount of hydrogen bonded CholHS, the side chains concentrate in a layer sandwiched between block copolymer domains. b) In the perpendicular smectic packing, found in samples with a high amount of hydrogen bonded CholHS, the side chains form smectic layers perpendicular to the block copolymer interfaces.

CholHS to pyridine, there is a single hydrogen bonded and nonbonded CholHS rich layer that is sandwiched between two layers of P2VP or P4VP (Figure 7a). This is the case of P4-25 and partially P4-50 as well as of all PBd-P2VP samples P2-40-P2-75 because the hydrogen bonding between CholHS and the P2VP repeat units is limited by steric hindrance as discussed earlier. The low attachment of CholHS leads to the side chains forming their own lamella inside the side chain block domain. The single layer packing is different from the smectic layers which are oriented parallel to block domain interfaces found in some side chain block copolymers after shear orientation³³ or roll casting.^{18,31} Instead, the single layer structure of Figure 7a seems not to be due to liquid crystalline type organization of the side chain blocks. Rather, it is a new type of self-assembly of side chain diblock copolymers resembling the microphase separation of linear triblock copolymers^{42–45} or certain types of supramolecular tailed-dendron systems.⁴⁶ Attached CholHS side chains act as “compatibilizers” that allow nonattached CholHS to be incorporated into the microphase separated structure preventing macrophase separation. In the P4-50 and P4-75 samples the hydrogen bonding of CholHS is high enough to promote the perpendicular smectic subphase schematically depicted in Figure 7b. The same subphase structures can be found for example in the PS-P4VP(CholHS) samples with high CholHS content by Korhonen et al.¹⁰ and in PMMA based diblock copolymers with covalent (every repeat unit carries a side chain) cholesterol side chains by Laiho et al. without shear alignment.³³ Thus, the binding of CholHS side chains to the host blocks plays a major role in the formation of the perpendicular smectic subphase.

The overall lamellar structure period a does not change significantly even though the total molecular mass of the PBd-P2VP copolymers increases with an increasing amount of CholHS as can be seen from Table 1. After the hydrogen bonding limit of CholHS is reached, additional CholHS dissolves into the CholHS rich layers as “free” mesogens increasing the volume fraction of the layers. To suppress the growth of the total lamellar period, the interfacial area between the CholHS and P2VP rich layers must increase proportionally. This dilutes the density of P2VP chains at the interface allowing the noncomplexed parts of the blocks less stretched configurations which decreases the thickness of the P2VP layers thus canceling out the increased volume fraction of the CholHS layer. Indeed, the following additional structural evidence can be advanced in support of this mechanism and the proposed schemes in Figure 7. In the single lamella ordering, the width of the poly(vinylpyridine) layers (black color in Figure 7a) should reflect a folded “cross-sectional” behavior of the host coil blocks (P2VP or P4VP), whereas in the perpendicular smectic ordering (Figure 7b), the total length of a host lamella domain (the black stripes in Figure 6a) should reflect a nearly fully stretched host chain, with a consequent large difference in feature sizes. From TEM, it is evident that there is a large aspect ratio (approximately five) between the length of the smectic lamellae of Figure 7b scenario (for example as in the case of P4-75, see Figure 6d) versus the width of individual black lamellae in the Figure 7a case (for example as in the case of P4-25, see Figure 6b), in agreement with expectations from the two proposed topological packing schemes. This behavior has been previously observed for example by Tenneti et al.³²

CONCLUSIONS

CholHS mesogens were hydrogen bonded to PBd-P2VP and PS-P4VP diblock copolymers. The pure copolymers microphase separated to hexagonally ordered P2VP cylinders in the PBd matrix or P4VP cylinders in the PS matrix. In P2-25, the morphology changed to perforated lamellar due to increased volume fraction of the P2VP(CholHS) block. Beside this specific case, the rest of the PBd-P2VP samples P2-40-P2-75 and all PS-P4VP(CholHS) samples exhibited a regular lamellar morphology. The hierarchical phase-separation of CholHS side chains followed a binding dependent behavior. In general, when the CholHS side chain binding to the host block was low, the CholHS mesogens concentrated in a single layer in the middle of the P2VP or P4VP lamellae. This subphase structure was found in P4-25 and in P2-40-P2-75 samples which can be considered as low attachment ratio samples. This is because, according to FTIR, hydrogen bonding of CholHS to the P2VP blocks was not complete as the attachment ratio saturated at around 0.3 according to the ratio between the absorption peaks at 1599 cm^{-1} and 1590 cm^{-1} . The saturation originated from steric hindrance effects caused by the unfavorable position of the hydrogen bonding nitrogen atom in the repeat units of P2VP. The low bonding of the side chains leads to this highly specific microphase separation scheme where the copolymer blocks and the CholHS mesogens simultaneously minimize their interaction with each other. In the high CholHS to P4VP repeat unit ratio sample, P4-75, the amount of hydrogen bonded CholHS side chains induced smectic layering of the side chain blocks and results in the observed perpendicular subphase. In the intermediate P4-50 sample, both the single CholHS layer and perpendicular smectic ordering could be found to coexist. It can be concluded that the structure of the subphase can be controlled by the attachment of CholHS side chains. The parallel orientation could be utilized for example to disperse compatibilized nanoparticles selectively in the middle of the side chain block domain.

The overall periodicities of the lamellar PBd-P2VP(CholHS) domains were between 24 and 26 nm. The invariance of the period in the higher amounts of CholHS containing samples in spite of an increased amount of CholHS can be explained by an increased interfacial area between the CholHS and P2VP rich layers and subsequent coiling of the P2VP chains. This was consistently assessed in block copolymers exhibiting both packing schemes (PS-P4VP), by comparing the characteristic feature sizes for the host block domains (P4VP), extracted by TEM, in both the single layer and perpendicular smectic subphases. It was thus found that the high aspect ratios between the P4VP length in the smectic layers, versus the width of the P4VP domains in the single CholHS layer case, are consistent with the proposed structural switching among the packing morphologies observed.

ASSOCIATED CONTENT

Supporting Information

The detailed synthesis and characterization of PBd-P2PV. This material is available free of charge via the Internet at <http://pubs.acs.org>.

AUTHOR INFORMATION

Corresponding Author

*E-mail: hadjichristidis@chem.uoa.gr (N.H.), janne.ruokolainen@aalto.fi (J.R.).

Notes

The authors declare no competing financial interest.

■ ACKNOWLEDGMENTS

We acknowledge the funding from the Academy of Finland (projects 128636, 140303, and 140362).

■ REFERENCES

- (1) Fischer, H.; Poser, S. *Acta Polym.* **1996**, *47*, 413–428.
- (2) Thomas, E. L.; Chen, J. T.; O'Rourke, M. J. E.; Ober, C. K.; Mao, G. *Macromol. Symp.* **1997**, *117*, 241–256.
- (3) Poser, S.; Fischer, H.; Arnold, M. *Prog. Polym. Sci.* **1998**, *23*, 1337–1379.
- (4) Ruokolainen, J.; Saariaho, M.; Ikkala, O.; ten Brinke, G.; Thomas, E. L.; Torkkeli, M.; Serimaa, R. *Macromolecules* **1999**, *32*, 1152–1158.
- (5) Ruokolainen, J.; ten Brinke, G.; Ikkala, O. *Adv. Mater.* **1999**, *11*, 777–780.
- (6) Thünemann, A. F.; General, S. *Macromolecules* **2001**, *34*, 6978–6984.
- (7) Bondzic, S.; de Wit, J.; Polushkin, E.; Schouten, A. J.; ten Brinke, G.; Ruokolainen, J.; Ikkala, O.; Dolbnya, I.; Bras, W. *Macromolecules* **2004**, *37*, 9517–9524.
- (8) Nandan, B.; Lee, C. H.; Chen, H. L.; Chen, W. C. *Macromolecules* **2005**, *38*, 10117–10126.
- (9) Chiang, W.; Lin, C.; Nandan, B.; Yeh, C.; Rahman, M. H.; Chen, W.; Chen, H. *Macromolecules* **2008**, *41*, 8138–8147.
- (10) Korhonen, J. T.; Verho, T.; Rannou, P.; Ikkala, O. *Macromolecules* **2010**, *43*, 1507–1514.
- (11) Anthamatten, M.; Hammond, P. T. *J. Polym. Sci., Part B: Polym. Phys.* **2001**, *39*, 2671–2691.
- (12) Shah, M.; Pryamitsyn, V.; Ganesan, V. *Macromolecules* **2008**, *41*, 218–229.
- (13) Potemkin, I. I.; Bodrova, A. S. *Macromolecules* **2009**, *42*, 2817–2825.
- (14) Fischer, H.; Poser, S.; Arnold, M.; Frank, W. *Macromolecules* **1994**, *27*, 7133–7138.
- (15) Fischer, H.; Poser, S.; Arnold, M. *Macromolecules* **1995**, *28*, 6957–6962.
- (16) Mao, G.; Wang, J.; Clingman, S. R.; Ober, C. K.; Chen, J. T.; Thomas, E. L. *Macromolecules* **1997**, *30*, 2556–2567.
- (17) Mao, G.; Wang, J.; Ober, C. K.; Brehmer, M.; O'Rourke, M. J.; Thomas, E. L. *Chem. Mater.* **1998**, *10*, 1538–1545.
- (18) Anthamatten, M.; Zheng, W. Y.; Hammond, P. T. *Macromolecules* **1999**, *32*, 4838–4848.
- (19) Osuji, C. O.; Chen, J. T.; Mao, G.; Ober, C. K.; Thomas, E. L. *Polymer* **2000**, *41*, 8897–8907.
- (20) Li, C.; Hsu, J.; Sugiyama, K.; Hirao, A.; Chen, W.; Mezzenga, R. *Macromolecules* **2009**, *42*, 5793–5801.
- (21) Anthamatten, M.; Hammond, P. T. *Macromolecules* **1999**, *32*, 8066–8076.
- (22) Yu, H.; Kobayashi, T.; Yang, H. *Adv. Mater.* **2011**, *23*, 3337–3344.
- (23) Hammond, M. R.; Mezzenga, R. *Soft Matter* **2008**, *4*, 952–961.
- (24) Bondzic, S.; Polushkin, E.; Ruokolainen, J.; ten Brinke, G. *Polymer* **2008**, *49*, 2669–2677.
- (25) Valkama, S.; Ruotsalainen, T.; Nykänen, A.; Laiho, A.; Kosonen, H.; ten Brinke, G.; Ikkala, O.; Ruokolainen, J. *Macromolecules* **2006**, *39*, 9327–9336.
- (26) Tsao, C. S.; Chen, H. L. *Macromolecules* **2004**, *37*, 8984–8991.
- (27) Naidu, S.; Ahn, H.; Lee, H.; Jung, Y. M.; Ryu, D. Y. *Macromolecules* **2010**, *43*, 6120–6126.
- (28) Ruokolainen, J.; Mäkinen, R.; Torkkeli, M.; Mäkelä, T.; Serimaa, R.; ten Brinke, G.; Ikkala, O. *Science* **1998**, *280*, 557–560.
- (29) Valkama, S.; Kosonen, H.; Ruokolainen, J.; Haatainen, T.; Torkkeli, M.; Serimaa, R.; ten Brinke, G.; Ikkala, O. *Nat. Mater.* **2004**, *3*, 872–876.
- (30) Osuji, C.; Chao, C.; Bitá, I.; Ober, C. K.; Thomas, E. L. *Adv. Funct. Mater.* **2002**, *12*, 753–758.
- (31) Zheng, W.; Albalak, R. J.; Hammond, P. T. *Macromolecules* **1998**, *31*, 2686–2689.
- (32) Tenneti, K. K.; Chen, X.; Li, C. Y.; Wan, X.; Fan, X.; Zhou, Q.; Rong, L.; Hsiao, B. S. *Macromolecules* **2007**, *40*, 5095–5102.
- (33) Laiho, A.; Hiekkataipale, P.; Ruokolainen, J.; Ikkala, O. *Macromol. Chem. Phys.* **2009**, *210*, 1218–1223.
- (34) Wojdyr, M. *J. Appl. Crystallogr.* **2010**, *43*, 1126–1128.
- (35) Takashi, H.; Mamola, K.; Plyler, E. J. *Mol. Spectrosc.* **1966**, *21*, 217–230.
- (36) Pouchert, C. J. In *The Aldrich Library of FT-IR Spectra*; Aldrich Chemical Company, Inc.: 1985.
- (37) Lee, J. Y.; Painter, P. C.; Coleman, M. M. *Macromolecules* **1988**, *21*, 954–960.
- (38) Stewart, D.; Imrie, C. T. *J. Mater. Chem.* **1995**, *5*, 223.
- (39) Alder, K.; Stewart, D.; Imrie, C. J. *J. Mater. Chem.* **1995**, *5*, 2225–2228.
- (40) Socrates, G. In *Infrared and Raman Characteristic Group Frequencies*; John Wiley & Sons Ltd.: Great Britain, 2001.
- (41) Matsuo, M.; Sagae, S.; Asai, H. *Polymer* **1969**, *10*, 79–87.
- (42) Mogi, Y.; Nomura, M.; Kotsuji, H.; Ohnishi, K.; Matsushita, Y.; Noda, I. *Macromolecules* **1994**, *27*, 6755–6760.
- (43) Stadler, R.; Auschra, C.; Beckmann, J.; Krappe, U.; Voight-Martin, I.; Leibler, L. *Macromolecules* **1995**, *28*, 3080–3097.
- (44) Bailey, T. S.; Pham, H. D.; Bates, F. S. *Macromolecules* **2001**, *34*, 6994–7008.
- (45) Schacher, F.; Yuan, J.; Schoberth, H. G.; Müller, A. H. E. *Polymer* **2010**, *51*, 2021–2032.
- (46) Merlet-Lacroix, N.; Rao, J.; Zhang, A.; Schlüter, A. D.; Bolisetty, S.; Ruokolainen, J.; Mezzenga, R. *Macromolecules* **2010**, *43*, 4752–4760.